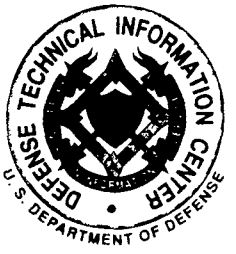

Defense Technical Information Center Compilation Part Notice

This paper is a part of the following report:

• *Title:* Technology Showcase: Integrated Monitoring, Diagnostics and Failure Prevention. Proceedings of a Joint Conference, Mobile, Alabama, April 22-26, 1996.

• *To order the complete compilation report, use:* AD-A325 558

The component part is provided here to allow users access to individually authored sections of proceedings, annals, symposia, etc. However, the component should be considered within the context of the overall compilation report and not as a stand-alone technical report.

FAILURE ANALYSIS OF MODULAR LIFT LINK, LUG MOUNTING, SELF-LOCKING NUTS

Scott Grendahl
U.S. Army Research Laboratory
Aberdeen Proving Ground, Aberdeen, MD

Abstract: The U.S. Army Research Laboratory-Materials Directorate (USARL-MD) conducted a failure analysis of two self-locking nuts from an army attack helicopter, at the request of the U.S. Army Aviation and Troop Command (ATCOM). Light optical and scanning electron microscopy were utilized to characterize the fracture halves of the broken nuts. The self-locking nuts are governed by Specification MS21042, *Nut, Self-Locking, 450°F, Reduced Hexagon, Reduced Height, Ring Base, Non-Corrosion Resistant Steel.* During phase maintenance on the lift beam in the pylon area, maintenance crews noticed the bolts securing the lift link support lug were not properly seated. Further inspection showed that the left side self-locking nuts were cracked and/or missing. The right side nuts were also cracked.

Key Words: Failure Analysis; Stress Corrosion Cracking (SCC); Hydrogen Assisted Cracking (HAC)

Visual Examination and Light Optical Microscopy: The two failed components were further designated as failures "A" and "B". Nut "A" was sectioned such that the fracture surfaces could be examined. The fracture origins were determined to be at the root of the first thread for both Nuts "A" and "B", and are shown in Figures 1 - 4 (arrows denote origins). Nut "B" contained two separate fracture surfaces, and subsequently both were examined. These two fracture surfaces of Nut "B" can be seen in Figures 3 and 4. They were further designated as fracture "B1" and "B2" for convenience. Note the radial lines which emanate from the fracture origins. The cadmium plating adjacent to the fracture surfaces was worn and damaged but no evidence of significant corrosion was observed. There was also no corrosion visible on the remaining fracture surfaces. A shear lip region was observed extending around one end of Nut "A", however no such failure mode was observed on Nut "B". In addition, beyond the third or fourth threads of both nuts the fracture morphologies revealed the direction of extrusion. This was evidenced by the sets of parallel lines (which represent grain flow) running perpendicular to the threads. The threads of both nuts were slightly damaged in that the tips of the threads were worn away, however this was determined to be post-fracture induced.

Metallographic Examination: The nuts were sectioned such that longitudinal (parallel to the thread direction) and transverse (perpendicular to the thread direction) specimens

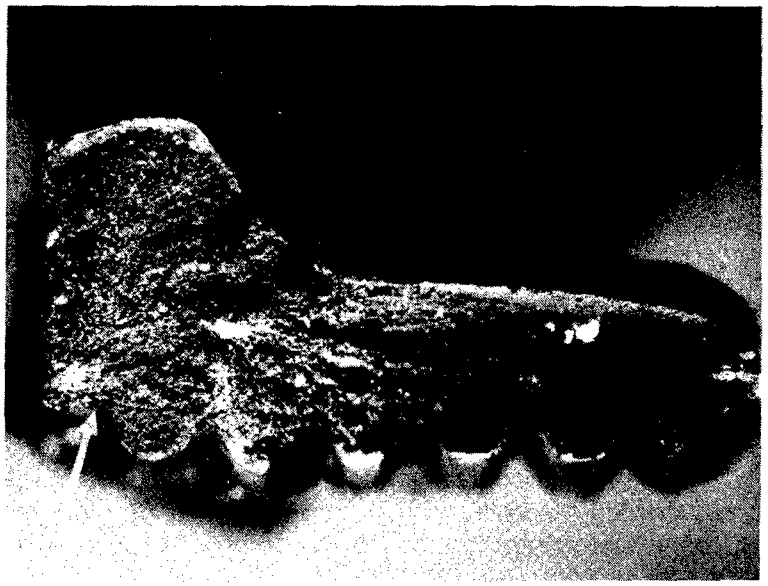

Figure 1. Micrograph of the fracture surface of Nut "A". Mag. 20x

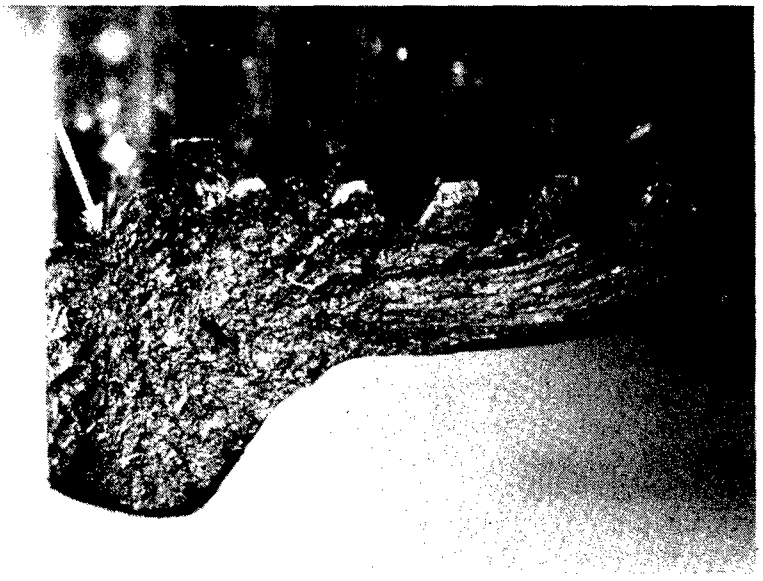

Figure 2. Micrograph of the mating fracture surface of Figure 7. Mag. 20x

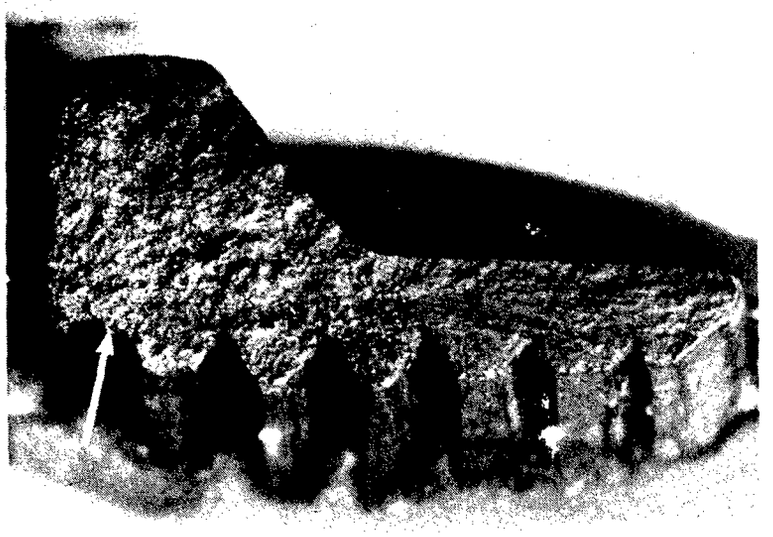

Figure 3. Micrograph of the fracture surface of Nut "B1". Mag. 20x

Figure 4. Micrograph of Nut "B" fracture surface "B2". Mag. 20x

were prepared. Metallographic preparation included mounting the samples in phenolic powder, rough polishing utilizing silicon carbide papers ranging from 240 to 600 grit, and fine polishing utilizing 3 micron alumina and 0.025 micron colloidal silica. No internal cracks were noted within the transverse or longitudinal specimens. Internal cracking is sometimes seen in HAC failures when it occurs within the plating bath. However, if the nuts failed primarily as a result of stresses induced during torquing, these internal cracks may be absent. The structures showed very fine martensitic lathe characteristics and were consistent with the prior heat treatment of the nuts.

Hardness Testing: The mounted samples were subjected to Knoop microhardness testing to determine conformance to the guideline of 49 HRC maximum (as required in Specification MS21042). Rockwell "C" scale readings could not be measured directly on the part due to geometric constraints, or on the mounted samples because of their small size. Therefore, Knoop readings were performed and converted to the Rockwell "C" scale. A total of five readings were taken on each sample. A load of 500 gmf was utilized. The results are listed in Table I and Table II. The converted hardness values conformed to the governing specification.

Table I. Nut "A"
HRc Hardness Values (Converted)
Knoop 500 gmf

Longitudinal	Transverse
48.8	49.0
47.8	48.3
48.6	48.7
48.5	48.1
48.2	48.3

Table II. Nut "B"
HRc Hardness Values (Converted)
Knoop 500 gmf

Longitudinal	Transverse
48.9	48.9
47.8	49.0
48.6	49.0
48.7	48.6
48.6	48.7

Chemical Analysis: Chemical analysis was performed to verify the elemental composition of the alloy. Specification MS21042 designates seven different alloys which may be used. The alloys listed were AISI C1035, C1042, 1050, 4027, 4037, 8630 and

8740. The carbon content was determined through combustion-infrared detection, the sulfur by combustion-automatic titration and all other elements through direct current plasma emission spectroscopy. The results compared most favorably with alloy AISI 8740, as shown in Table III. However, the carbon content of Nut "B" and the sulfur content of Nut "A" each slightly exceeded the maximum limits set forth in AISI 8740. This nonconformity suggested a possible lack of melt control. The minute additional amounts of carbon and sulfur would most likely have no adverse affects on mechanical properties, and were considered negligible.

Table III.
Chemical Analysis
Weight Percent

lem.	Nut A	Nut B	C1035	C1042	1050	4027	4037	8630	8740
	0.439	0.4[illegible]	0.31-0.38	0.40-0.47	0.47-0.55	0.25-0.30	0.35-0.40	0.28-0.33	0.38-0.44
in	0.84	0.88	0.60-0.90	0.60-[illegible].90	0.60-0.90	0.70-[illegible].90	0.70-0.90	0.70-0.90	0.75-1.00
i	0.30	0.031	0.15-0.35	0.3 max	0.3 max	0.15-0.35	0.15-0.35	0.15-0.35	0.15-0.35
	0.018	0.020	0.04 max	0.04 max	0.04 max	0.035max	0.035max	0.025max	0.025max
	0.026	0.022	0.05 max	0.05 max	0.05 max	0.04 max	0.04 max	0.025max	0.025max
r	0.55	0.57	*	*	*	*	*	0.40-0.60	0.40-0.60
li	0.46	0.50	*	*	*	*	*	0.40-0.70	0.40-0.70
lo	0.21	0.21	*	*	*	0.20-0.30	0.20-0.30	0.15-0.25	0.20-0.30
u	0.079	0.085	*	*	*	*	*	0.35 max	0.35 max
e	rem.	rem.	rem.	rem.	rem.	rem.	rem.	rem.	rem.

Scanning Electron Microscopy and EDS: The fractures of Nut "A" and Nut "B" were classic cases of HAC with service stress related failure. SEM fractographs of Nut "A" and "B" failures are shown in Figures 5, 6 and 7, 8 respectively. The fracture morphologies at the crack origins of Nuts "A" and "B" were intergranular (I) as shown in Figures 9 and 10. These SEM micrographs show the traditional "rock candy" features, as well as some secondary cracking. X-ray mapping (utilizing energy dispersive spectroscopy) of the entire fracture surfaces did not reveal a layer of cadmium on or near the fracture origins. The absence of a cadmium film suggests the cracking most likely occurred in service rather than in the plating bath. The intergranular regions transitioned to large mixed-mode (D/I) regions consisting of intergranular decohesion and ductile dimples covering nearly half of the fracture surfaces. These mixed mode morphologies are shown in Figures 11 and 12. The mixed-mode morphologies transitioned abruptly to ductile dimples (D) as shown in Figures 13 and 14. This abrupt change in morphology represents the areas of fast fracture beyond the third or fourth threads. Figures 13 and 14 also show the ductile dimples aligned in the extrusion direction of the components. Shear lips (SL) were also noted on Nut "A", indicative of the last region to fail. Light optical and scanning electron microscopy did not reveal any gross anomalies at the fracture origin. The schematics shown in Figure 15 and 16 outline the different

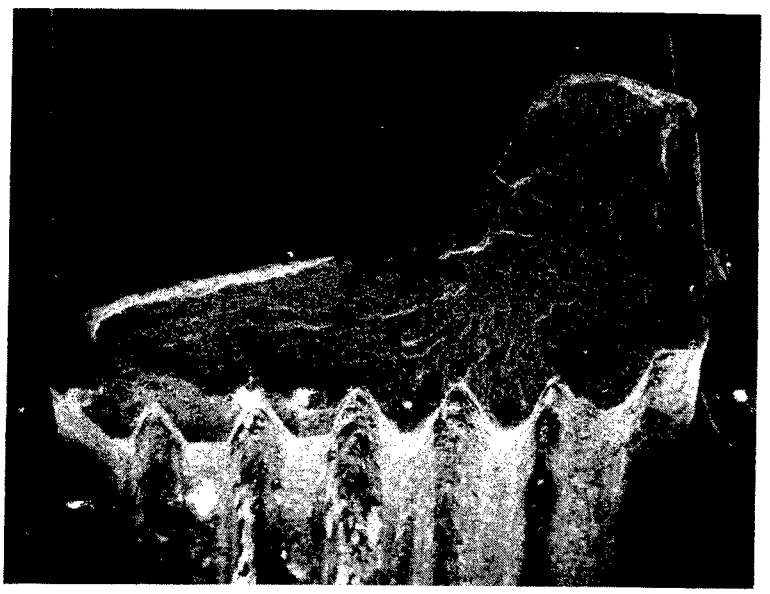

Figure 5. SEM micrograph of the fracture surface of Nut "A". Mag. 15x

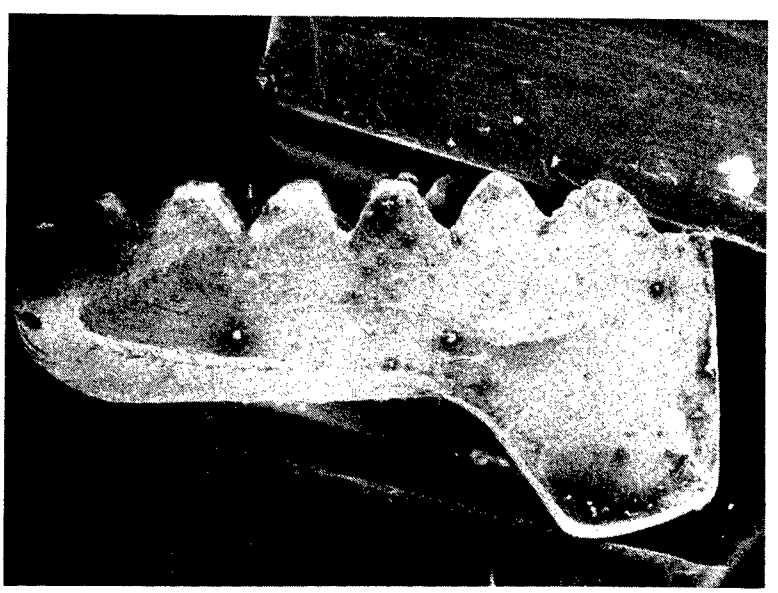

Figure 6. Mating fracture surface of Nut "A" Figure 19. Mag. 15x

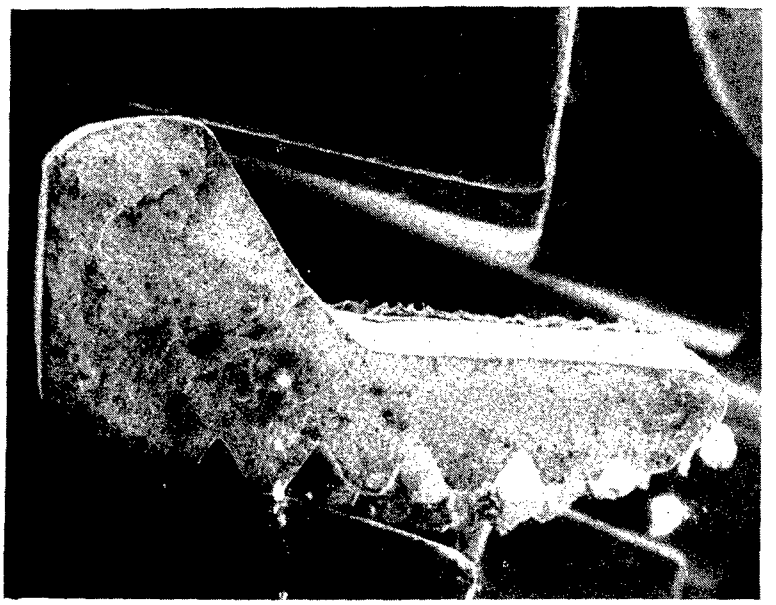

Figure 7. SEM micrograph of the fracture surface of specimen "B1". Mag. 15x

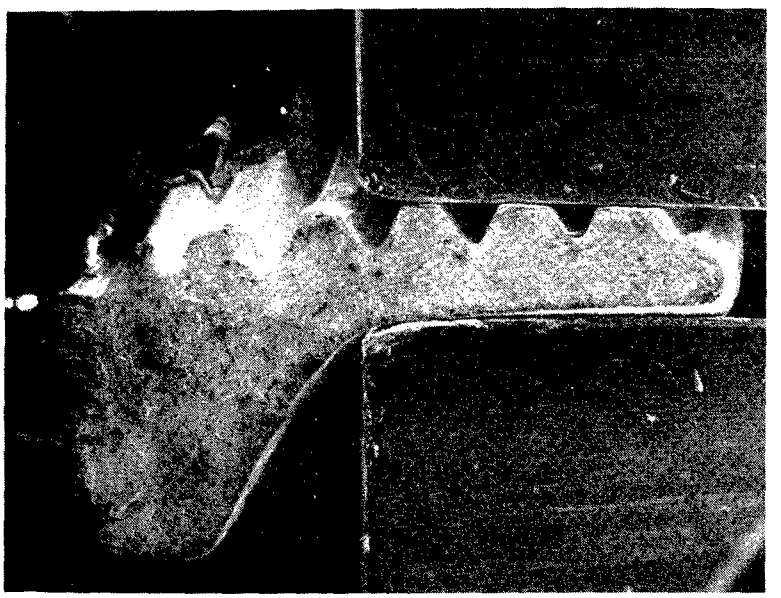

Figure 8. SEM micrograph of the fracture surface of specimen "B2". Mag. 15x

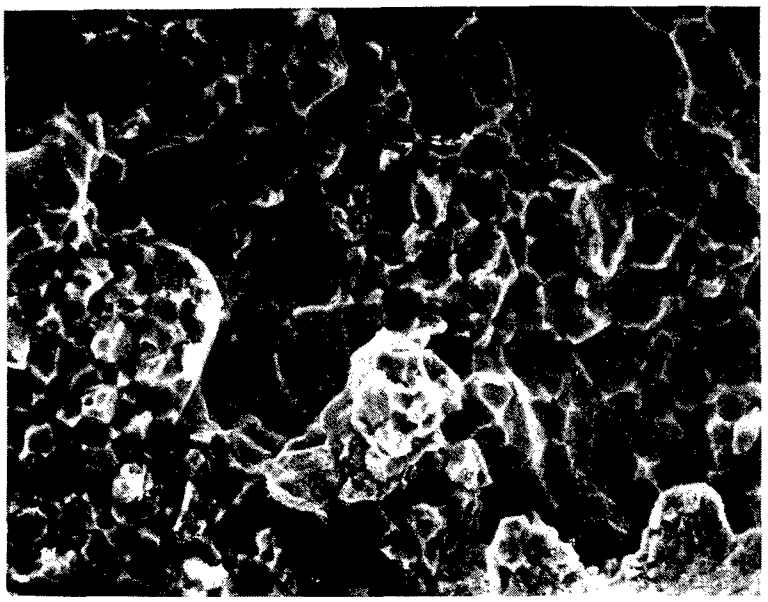

Figure 9. SEM fractograph of morphology at the origin of Nut "A". Mag. 1000x

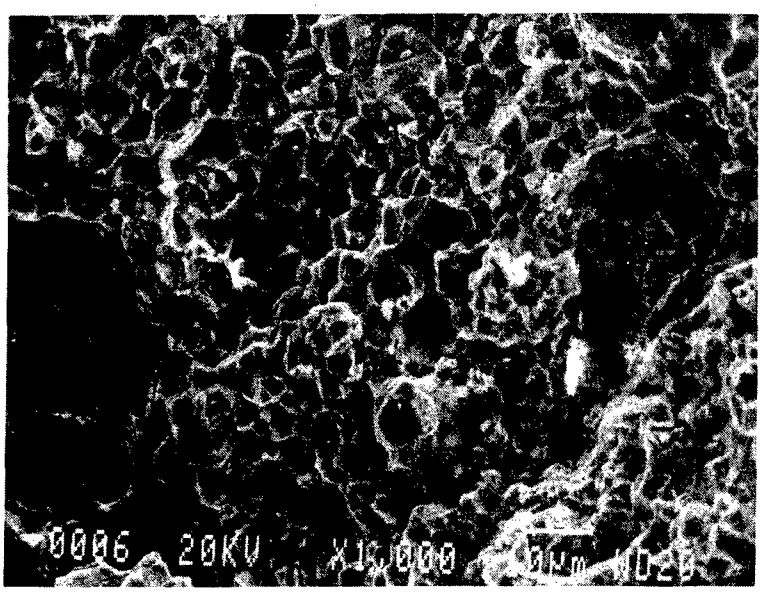

Figure 10. SEM fractograph of morphology at the origin of Nut "B". Mag. 1000x

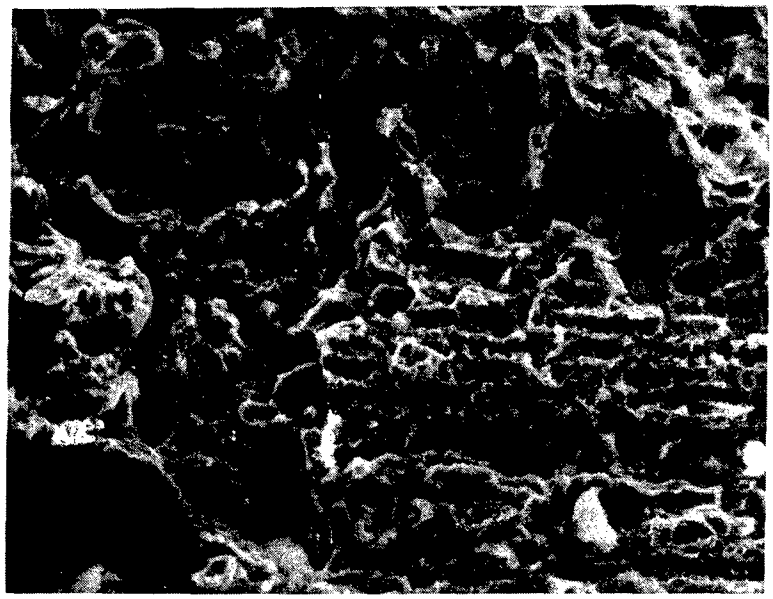

Figure 11. SEM fractograph of mixed-mode morphology of Nut "A". Mag 1000x

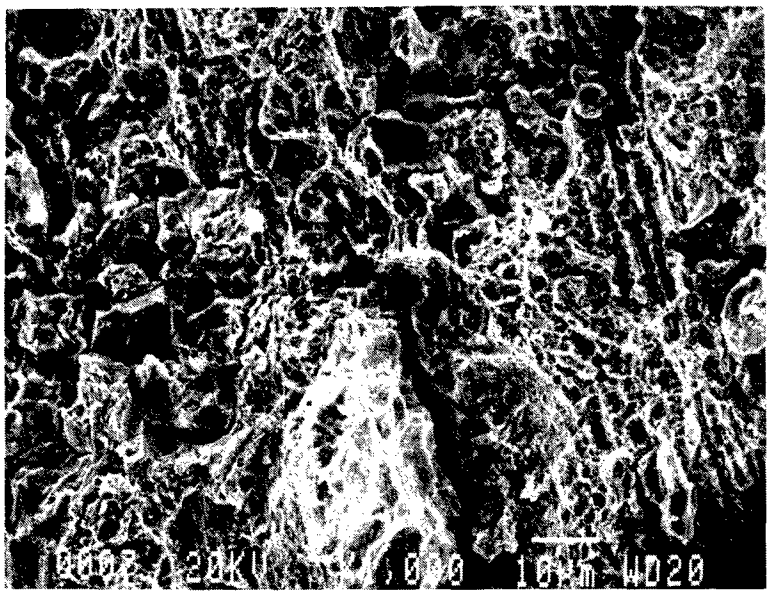

Figure 12. SEM fractograph of mixed-mode morphology of Nut "B". Mag 1000x

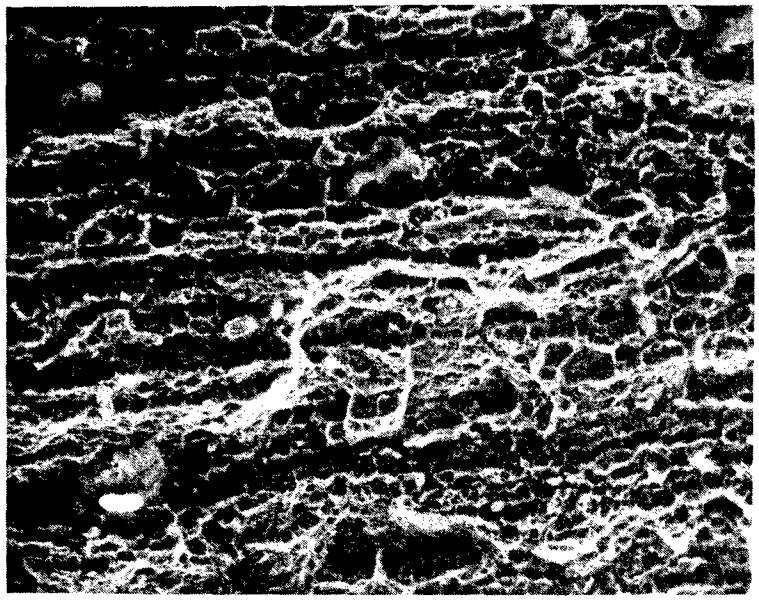

Figure 13. SEM fractograph of ductile dimple morphology of Nut "A". Mag 1000x

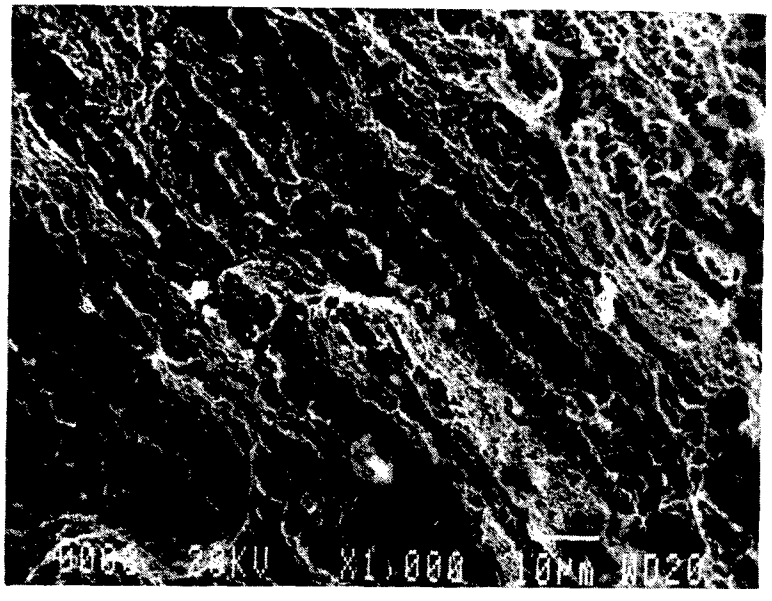

Figure 14. SEM fractograph of ductile dimple morphology of Nut "B". Mag 1000x

morphologies noted on the mating fracture surfaces of Nut "A" and the two different fracture surfaces of Nut "B", respectively.

Discussion: A part subjected to stress corrosion cracking (SCC) exhibits a fracture morphology similar to that noted in this investigation. However, the lack of corrosion and corrosion products on or near the fracture surfaces and the lack of significant crack branching ruled out SCC as a failure mode. Therefore, the failure was attributed to hydrogen assisted cracking. The most likely source of the hydrogen in the fabrication of this component was the cadmium plating process. Specification QQ-P-416 is an electro-deposition plating method, which creates nascent hydrogen that diffuses into the parts during plating. A post-bake is recommended for high strength steels to prevent hydrogen embrittlement. Baking subsequent to plating is required for moderate to high strength steels, usually at 375°F within four hours of plating to evenly disperse the hydrogen which had diffused into the component. Baking time is usually dependent on the strength of the component and the geometry of the part. Problems of embrittlement can arise if the parts are a) plated in an improper bath, b) not post-baked, c) post-baked after a prolonged period of time after the plating process, or d) post-baked at an incorrect temperature or bake time. It is well documented that the absorption of hydrogen into a steel results in a loss of ductility over a sustained stress. However, this could not be substantiated by ARL-MD since tensile specimens could not be fabricated due to the small size of the failed components.

Conclusion: The self-locking nuts under investigation failed as a result of hydrogen assisted cracking (HAC). The primary source of the hydrogen would most likely have been related to a manufacturing operation (electro-deposited cadmium plating) as opposed to the service environment. Evidence substantiating this conclusion was the intergranular mode of fracture and the absence of corrosion on the fracture surfaces. The service life of these components was not known. However, it is possible that the nuts may have been broken for some time before the failures were discovered. ARL-MD has experienced HAC related failures associated with the manufacturer of these nuts and its cadmium plating procedures in the recent past. The nuts were cadmium plated (electro-deposited) in accordance with QQ-P-416, Type II, Class 2 per specification MS21042. These nuts also had a hardness between 48-49 HRc, which converts to a UTS between 238-246 KSI. It is important to note that QQ-P-416 Rev. F does not recommend electro-plating parts with a UTS above 200 KSI, because of the susceptibility of high strength steels to embrittle from nascent hydrogen.

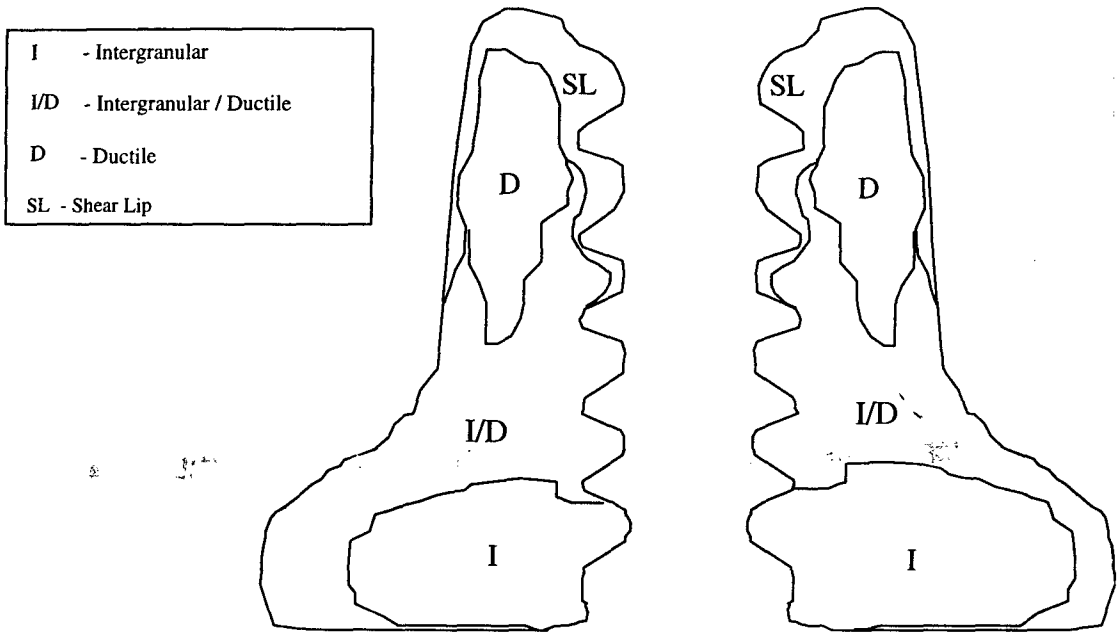

Figure 15. Map of failure modes for mating fracture halves of Nut "A"

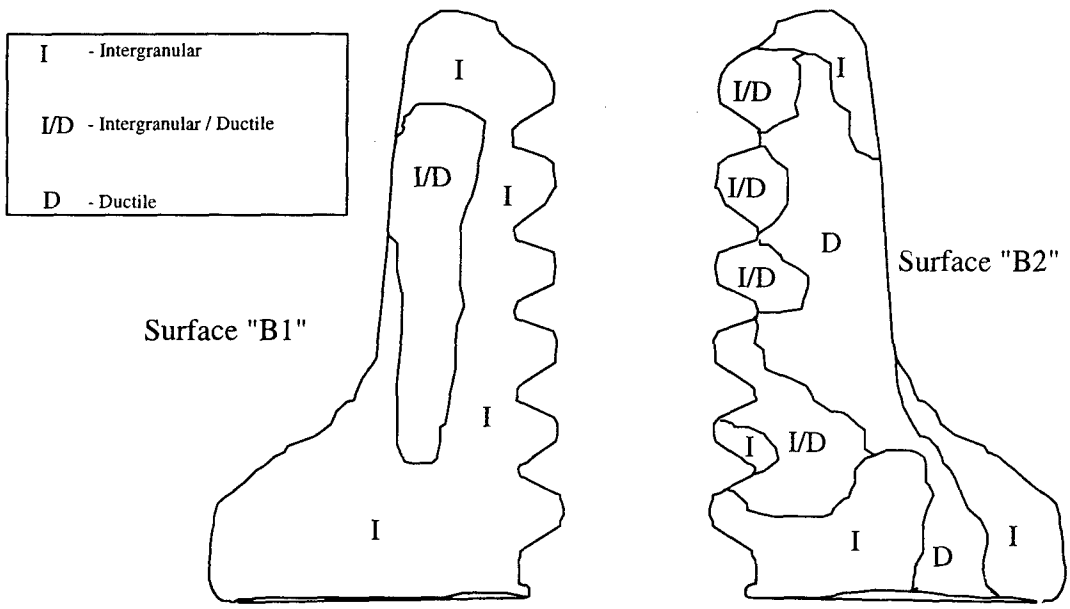

Figure 16. Map of failure modes of fracture surfaces of Nut "B"